Journal of Fluorine Chemistry 131 (2010) 751–760

Contents lists available at ScienceDirect

Journal of Fluorine Chemistry

journal homepage: www.elsevier.com/locate/fluor

Experimental and chemical kinetic study of the pyrolysis of trifluoroethane and the reaction of trifluoromethane with methane

Wenfeng Han [a], Eric M. Kennedy [a,*], Sazal K. Kundu [a], John C. Mackie [a], Adesoji A. Adesina [b], Bogdan Z. Dlugogorski [a]

[a] Process Safety and Environment Protection Research Group, School of Engineering, The University of Newcastle, Callaghan, NSW 2308, Australia
[b] Reactor Engineering and Technology Group, School of Chemical Sciences and Engineering, University of New South Wales, Sydney, NSW 2052, Australia

ARTICLE INFO

Article history:
Received 11 February 2010
Received in revised form 15 March 2010
Accepted 19 March 2010
Available online 27 March 2010

Keywords:
HFC 23
CHF_3
Greenhouse gas
Vinylidene fluoride
Hydrofluorocarbon
Kinetic modelling

ABSTRACT

A detailed reaction mechanism is developed and used to model experimental data on the pyrolysis of CHF_3 and the non-oxidative gas-phase reaction of CHF_3 with CH_4 in an alumina tube reactor at temperatures between 873 and 1173 K and at atmospheric pressure. It was found that CHF_3 can be converted into C_2F_4 during pyrolysis and $CH_2{=}CF_2$ via reaction with CH_4. Other products generated include C_3F_6, CH_2F_2, C_2H_3F, C_2HF_3, C_2H_6, C_2H_2 and CHF_2CHF_2. The rate of CHF_3 decomposition can be expressed as $5.2 \times 10^{13}\,[s^{-1}]\,e^{-295[kJ\,mol^{-1}]/RT}$. During the pyrolysis of CHF_3 and in the reaction of CHF_3 with CH_4, the initial steps in the reaction involve the decomposition of CHF_3 and subsequent formation of CF_2 difluorocarbene radical and HF. It is proposed that CH_4 is activated by a series of chain reactions, initiated by H radicals. The NIST HFC and GRI-Mech mechanisms, with minor modifications, are able to obtain satisfactory agreement between modelling results and experimental data. With these modelling analyses, the reactions leading to the formation of major and minor products are fully elucidated.

1. Introduction

Global production and use of chlorofluorocarbons (CFCs) and halons has decreased significantly as a result of the phase out schedules of the 1987 Montreal Protocol and its subsequent amendments and adjustments [1]. The consumption and emission of hydrofluorocarbons (HFCs) are projected to increase substantially in the coming decades in response to regulation and replacement of ozone depleting gases under the Montreal Protocol [2].

Trifluoromethane (CHF_3, HFC-23, fluoroform, FE-13, R23) is an unintentional by-product generated during the manufacture of $CHClF_2$ (HCFC-22), and has limited application as a refrigerant or as a raw material for other products. It has a global warming potential 11,700 times greater than carbon dioxide and an atmospheric lifetime of 264 years. It is reported that the concentration of CHF_3 is steadily increasing in the atmosphere since at least 1978 at a present rate of increase of 5% per year [3].

Thus, the development of suitable methods for the treatment of CHF_3 is of great practical significance. However, limited research has focused on the development of treatment processes specifically for CHF_3, especially in comparison with the intensive research on technologies for destruction of halons or CFCs. One method, thermal oxidation, is a demonstrated technology for the destruction of CHF_3 as outlined in United Nations Framework Convention on Climate Change (UNFCCC) [4]. In this process, steam, O_2 and natural gas are used as reactants or fuels for the decomposition of CHF_3 at temperatures as high as 1473 K. It is also reported that phosphates and ZrO_2–SO_4 are active and stable catalysts for the destruction of CHF_3 in the presence of O_2 and steam at relatively low temperatures [5,6]. One of the problems with oxidation is that the fluorine has to be removed as HF from the exhaust gas stream and then recycled or disposed of as a fluoride salt. More recently, Moon et al. investigated the pyrolysis of a mixture of CHF_3 and tetrafluoroethylene (TFE) as a potential route for the production of hexafluoropropene (C_3F_6) and found that the addition of CHF_3 can significantly increase the yield of C_3F_6 compared to the pyrolysis of TFE alone [7].

In a previous work, we reported that CHF_3 can be converted to vinyl difluoride (VDF, $CH_2{=}CF_2$), a highly valuable feedstock, through reaction with CH_4, although the conversion and yield of target product were relatively low [8,9]. VDF is widely used as a fluoroelastomer which is a key monomer for the synthesis of a variety of products, most notably poly-(vinylidene fluoride) (PVDF), Viton (produced by Dupont Corporation), KEL-F (produced by 3M) and Aflas (produced by Asahi Glass Co. Ltd.). Components fabricated from fluoroelastomers enhance reliability, safety, and environmental friendliness in such areas as automotive and air transportation, the chemical processing industries, and in power generation [10]. A wide range of fluoroelastomer products have been developed to meet performance requirements in many

* Corresponding author. Tel.: +61 2 4985 4422; fax: +61 2 4921 6893.
E-mail address: eric.kennedy@newcastle.edu.au (E.M. Kennedy).

0022-1139/$ – see front matter © 2010 Elsevier B.V. All rights reserved.
doi:10.1016/j.jfluchem.2010.03.012

hostile environments, and to attain fabrication characteristics comparable to other elastomers. More recently, VDF was found to be an excellent source for the preparation of paints for high performance external architectural coatings [11].

The motivation of this study is to compare the thermal decomposition of CHF_3 alone and in the presence of CH_4. The conversion approach adopted in this work is distinctly different to conventional destruction processes, as we aim not to destroy fluoroform but rather to transform it to a useful product. Through the combination of experimental work and kinetic modelling simulation presented in this manuscript, the elementary reactions dominating CHF_3 decomposition, CH_4 activation and the formation of products can be fully elucidated.

2. Experimental

The pyrolysis of CHF_3 and reaction of CHF_3 with CH_4 was carried out in a tubular alumina reactor with an inner diameter of 7.0 mm. This experimental facility has been described in detail elsewhere [12,13]. Briefly, the apparatus consists of a tubular high purity (99.99%) alumina reactor. Carbon containing products were identified by a GC/MS (Shimadzu QP5000) equipped with an AT-Q column, and quantified with a micro-GC (Varian CP-2003) equipped with molecular sieve 5A and PoraPLOT Q columns. Relative molar response (RMR) factors of hydrocarbons and halogenated compounds for TCD detection were experimentally obtained from standard gas mixtures where possible. The RMR of species where standard gas mixture were not available were estimated from published correlations [14]. HF formed during the reaction was trapped with 0.1 M NaOH solution, and concentrations were determined by an ion chromatograph (IC) (Dionex-100) equipped with an IonPAS14A column (4 mm × 250 mm).

The gases and solid reactants used in this study include CHF_3 (>98%, Coregases), CH_4 (99.99%, Linde) and AlF_3 (Sigma, >99%). In reactions which involved AlF_3, 0.2 g aluminium fluoride was charged into the uniform zone of the reactor, and held in place by alumina chips (99.99%). Prior to reaction, aluminium fluoride was dried in situ in a nitrogen atmosphere (99.999%, Linde) for 2 h at 673 K and 1.5 h at 1073 K. Feed gases, diluted in nitrogen (99.999%, Linde), were introduced to the reaction zone.

3. Chemical kinetic modelling

The pyrolysis of CHF_3 and reaction of CHF_3 with CH_4 have been modelled using the commercial software package Cosilab [15]. During simulations, the steady state material balance for each species was performed. As all experiments were conducted under essentially isothermal conditions, energy balances were not undertaken. Successive grids tolerance for species profiles were set to 0.001(GRAD parameter) for species concentration and to 0.01 for the concentration gradients (CURV parameter). The final grids contained 150 mesh points. The kinetic mechanism and thermodynamic database used for reaction of fluorinated species was the NIST HFC mechanism [16] with oxygen chemistry deleted since there is no oxygen in the reacting systems. Gas Research Institute GRI-Mech [17] was used for the pyrolysis of CH_4, again with oxygen-containing species removed. For reaction of CHF_3 with CH_4, NIST HFC mechanism and GRI-Mech were combined and called GRI-NIST mechanism in this study.

Generally, a reasonable agreement of predictions of NIST HFC, GRI-Mech and GRI-NIST mechanisms for CHF_3 pyrolysis, CH_4 pyrolysis and reaction of CHF_3 with CH_4 with experimental data was obtained. However, deviations between experimental data and modelling predictions were found in some cases. Modifications to the mechanisms are suggested, and discussed.

4. Results and discussion

4.1. Thermal pyrolysis of CHF_3

In order to investigate the pyrolysis of CHF_3, the conversion of CHF_3 at temperatures from 973 to 1073 K and at 1.01 bar versus residence time was studied. Under these conditions, the conversion level of CHF_3 in a 10% CHF_3-90% N_2 pyrolysis mixture is generally below 10%. Hence, reaction rate of this diluted mixture can be approximated as

$$-r_A = kC_A^n \tag{1}$$

which integrates to

$$\ln\frac{1}{1-X} = kt \tag{2}$$

for a first-order ($n = 1$) mechanism, or

$$\frac{X}{1-X} = C_{Ao}kt \tag{3}$$

for a second-order ($n = 2$) mechanism.

Where k is the reaction rate constant ($(\text{mol cm}^{-3})^{1-n}\,\text{s}^{-1}$), C_A is the concentration of CHF_3 (mol cm^{-3}), r_A is the rate of the reaction (mol $\text{cm}^{-3}\,\text{s}^{-1}$), X is the conversion of CHF_3 and t reaction time.

We evaluate the pyrolysis kinetics of CHF_3, assuming ideal plug-flow conditions and a constant density system. The first-order and second-order equations were used to fit the experimental data and first-order assumption best matches the experimental data, as shown in Fig. 1. The apparent rate constants for CHF_3 decomposition in the temperature range from 973 to 1073 K, based on a least-squares fitting of the experimental rate constants with an Arrhenius expression is shown in Fig. 1. The rate constant expression for the first-order reaction is given by;

$$k = 5.2 \times 10^{13}\,[\text{s}^{-1}]\,\text{e}^{-295\pm46\,[\text{kJ mol}^{-1}]/RT} \tag{4}$$

The pyrolysis of CHF_3 was first studied using shockwave techniques in the temperature range of 1200–1600 K [18,19]. Since then, various results have been reported based on shock wave experiments [20–22] or RRKM theoretical calculations [23]. These derived rate expressions are summarized in Table 1, along with the pressures and temperatures under which the data were obtained. It is generally agreed that the initial step in the decomposition of CHF_3 is the dehydrofluorination and formation of CF_2 species. We will discuss the reactivity of singlet and triplet states of CF_2 in more detailed in Section 4.2.2.

As shown in Table 1, the values of A and E_a obtained from our experimental data are close to the results of Placzek et al.'s RRKM calculation [23] and Politanskii et al.'s thermal pyrolysis experiments [24]. However, these rate constants are significantly lower than those reported by Tschuikow-Roux et al. [18,19]. Biordi et al. [25] studied the flame structure of bromotrifluoromethane-inhibited methane flames and found that the rate expressions given by Tschuikow-Roux et al. were too large to be consistent with low-pressure flame data. Using similar experimental techniques, an even lower activation energy for CHF_3 decomposition was suggested by Modica et al. behind incident and reflected shock waves over a temperature range from 1600 to 2200 K [20]. One possible reason for this discrepancy, as acknowledged by Tschuikow-Roux et al. [18], is the difficulty to appreciably vary the reaction dwell time while maintaining constant reaction temperature and pressure conditions in the single-pulse shock tube. Another reason for the discrepancy is that the decomposition of CHF_3 may be pressure-dependent and lie in the fall-off region near the second-order limit [19].

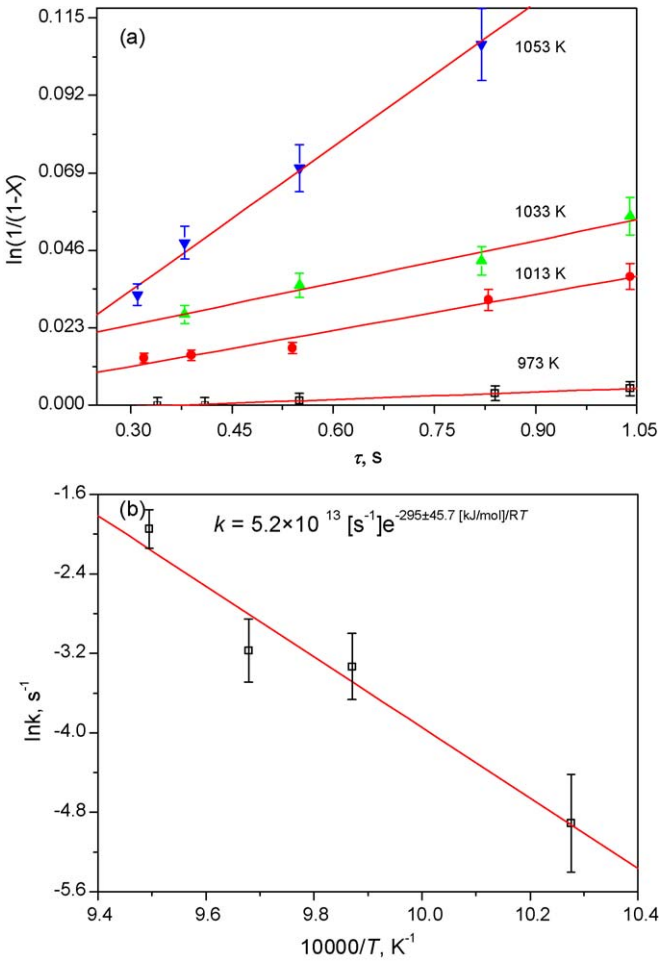

Fig. 1. (a) Apparent 1st order behavior for the pyrolysis of CHF_3 over the temperature range 973–1053 K. *X* represents fractional conversion of CHF_3. (b) Arrhenius plot for first-order reaction rate constant for the pyrolysis of CHF_3.

At pressures between 0.29 and 28.5 bar, Modica et al. found that the decomposition reaction was first order in CHF_3 concentration [20]. For the lowest pressure (0.29 bar), the reaction could also be interpreted by a second-order mechanism. Unfortunately, the calculated results did not reproduce the observed pressure dependence of the rates for the decomposition of fluoroform [23].

To explain the second-order mechanism, the following reactions were suggested [19]:

$$CHF_3 + M \rightleftarrows M + CHF_3^* \quad (R1)$$

$$CHF_3^* \rightarrow CF_2 + HF \quad (R2)$$

As C_2F_4 was observed as the major product in their experiments, Tschuikow-Roux et al. suggested that the vibrationally excited $C_2F_5H^*$ disproportionates rapidly into C_2F_4 plus HF. However, we suggest that reactions (R3a) and (R3b) play a relatively minor role under our experimental conditions, as there does not appear to be any reported observations of CF_2 insertion into CHF_3, and no evidence was found for CF_2 inserting into C–H of CH_4 or C_2H_4 over the temperature range of 295–873 K [26]. According to our quantum chemical calculations, it is found that CF_2 can insert into C–H of CH_4 with an activation energy as high as 163 kJ mol^{-1}. The exponential factor was estimated to be only 1.5×10^{11} cm^3 mol^{-1} s^{-1}. As argued in the reference [21], if reaction (R3a) is responsible for the consumption of CHF_3, we would anticipate the formation of CF_4, CF_2H_2, C_2F_6, $C_2F_4H_2$ and C_2F_5H, as a result of the following reactions:

$$CHF_3 + CF_2 \rightarrow CF_3 + CHF_2 \quad (R4)$$

$$CHF_3 + CF_3 \rightarrow CF_4 + CHF_2 \quad (R5)$$

$$CHF_3 + CHF_2 \rightarrow CF_3 + CH_2F_2 \quad (R6)$$

$$CF_3 + CF_3 \rightarrow C_2F_6 \quad (R7)$$

$$CHF_2 + CHF_2 \rightarrow C_2H_2F_4 \quad (R8)$$

$$CHF_2 + CF_3 \rightarrow C_2F_5H + M \quad (R9)$$

Furthermore, thermal decomposition of CHF_3 can be simulated very well when reaction (R3) is excluded [7,8,21]. Further investigations were undertaken to elucidate the mechanism of CHF_3 pyrolysis reaction and to estimate their associated kinetics parameters.

A feed mixture of N_2 and CHF_3, in which CHF_3 was approximately 10% by volume, was investigated at temperature range of 873–1173 K and at atmospheric pressure. The residence time was maintained at around 0.5 s by adjusting the volume of the reaction zone. The conversion of CHF_3 and the rate of product formation as a function of temperature are shown in Fig. 2. It is seen that CHF_3 pyrolysis commences around at 973 K at residence time of 0.5 s, and its conversion increases with temperature. At a temperature of 1173 K, 80% conversion of CHF_3 was achieved.

The products of CHF_3 pyrolysis detected by GC–MS analysis include C_2F_4, C_3F_6 and trace amounts of C_2HF_3 at higher temperatures. At temperatures above 1073 K, trace amounts of carbonaceous material were formed on the inner surface of the reactor. As a consequence, the carbon balance drops from 98% at 973 K to around 80% at 1173 K. Fig. 2(b) and (c) shows the formation rate of major products as a function of temperature. The production of C_2F_4 increases with temperature until 1133 K, at this temperature, a maximum formation rate is achieved before it decreases at temperatures higher than 1133 K. However, C_3F_6 formation commences at 1073 K and increases monotonically with

Table 1
Comparison of kinetic data of CHF_3 decomposition obtained in this study with references[a].

T (K)	Pressure (Pa)	*A* (s^{-1} or cm^3 mol^{-1} s^{-1})	*n*	*E* (kJ mol^{-1})	Reaction order	Ref.
1500–2000	4.93×10^3–4.93×10^5	1.29×10^{14}		302	1	[22]
1020–1320		2.75×10^{13}		289	1	[24]
1600–2200	2.93×10^4–2.93×10^6	7.03×10^{11}		244	1	[20]
1200–1600	3.07–4.27×10^5	1.26×10^{12}		264	1	[18]
1200–1600	9.12×10^4–1.89×10^6	1.00×10^{14}		249	1	[19]
600–2200		9.44×10^{13}		294	1	[23]
973–1073	1.01×10^5	5.2×10^{13}		295	1	This study
1150–1570	1.52–2.64×10^5	2.16×10^{-8}		244	2	[21]
1600–2200	2.93×10^4–2.93×10^6	2.01×10^{-3}	−5.75	244	2	[20]
600–2200		1.18×10^{-5}		269	2	[23]

[a] The rate coefficients of the forward reaction is $k = AT^n \exp(-E/RT)$, where *A* is in pre-exponential factor, *E* is activation energy and *R* is the ideal gas constant.

temperature. At temperatures above 1133 K, its formation rate exceeds that of C_2F_4.

The pyrolysis of CHF_3 was modelled using the NIST mechanism and a comparison of experimental data and predicted reactions is shown in Fig. 2. CHF_3 conversion levels agree reasonably with NIST predictions, although the levels observed experimentally are slightly higher than those predicted. The NIST mechanism predicts C_2F_4 as the sole carbon containing product species and the predicted rate of formation is consistent with the experimental results at temperatures below 1093 K. However, it is over-predicted significantly at temperatures above 1093 K and another major product, C_3F_6 which is detected experimentally is not included as a reaction product in this mechanism. In order to improve the model's consistency with experimental data, the NIST mechanism was modified by incorporating relevant kinetic data from the open literature. Initially, the kinetics parameters (*A* factor and activation energy) of reaction (R2) was replaced by Schug et al.'s parameters [22] as shown in Table 1. Similarly to the conclusions by Biordi et al. [25], these rate parameters appear to be too high for the pyrolysis of CHF_3 compared with experimental results. The kinetics parameters derived from our experiments, together with other reported studies, were added to NIST mechanism to produce a modified mechanism (see Table 2).

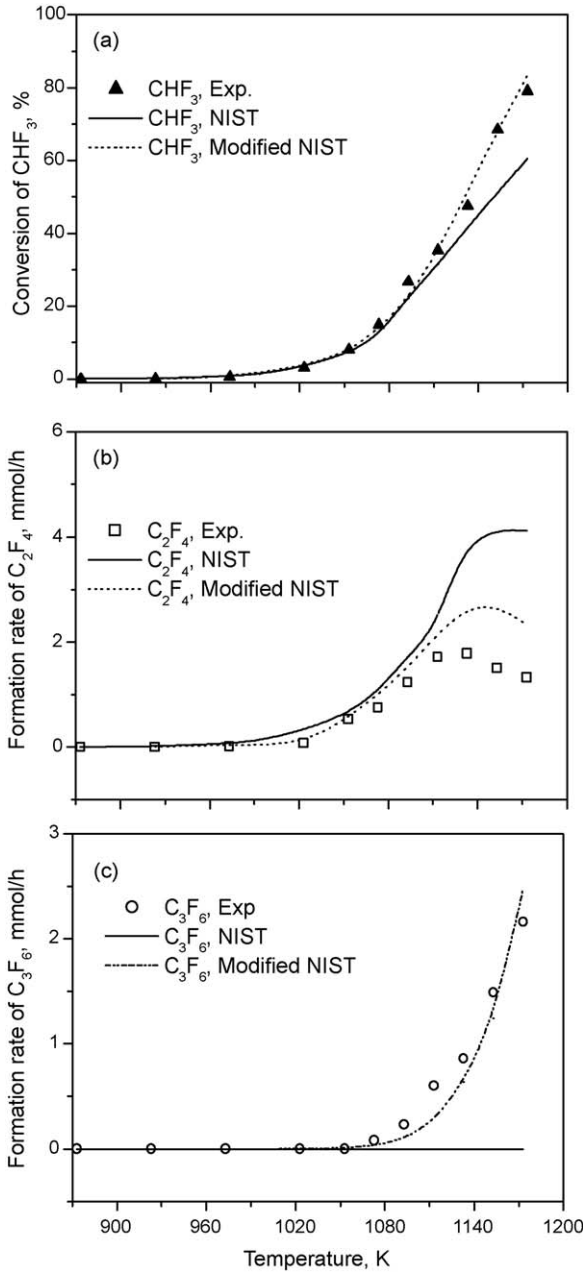

Fig. 2. Conversion of CHF_3 (a), rate of formation of C_2F_4 (b) and rate of formation of C_3F_6 (c) as a function of temperature during the pyrolysis of CHF_3.

$$CF_2 + CF_2{:}\ CF_2 \rightarrow C_3F_6 \quad \text{(R10)}$$

$$CF_2{:}\ CF_2 + CF_2{:}\ CF_2 \rightarrow C_3F_6 + CF_2 \quad \text{(R11)}$$

$$c\text{-}C_3F_6 \rightarrow CF_2{:}\ CF_2 + CF_2 \quad \text{(R12)}$$

$$c\text{-}C_3F_6 \rightarrow C_3F_6 \quad \text{(R13)}$$

In the CHF_3 pyrolysis mechanism, the initial reaction step involves the dehydrofluorination of CHF_3, resulting the formation of HF and CF_2 di-radical. Reactions (R3a) and (R3b) are not included in the mechanism since they are not likely to be responsible for the consumption of CHF_3 as discussed early. One clear deficiency of the existing mechanism is the absence of reaction pathways which lead to the formation of C_3F_6, and as such reactions (R10)–(R13) are introduced and are part of the modified mechanism. C_3F_6 also can be formed via reactions (R14)–(R17), but we suggest these are not primary pathways as the *A* factor for the formation of C_4F_8 ((R14) and (R15)) is as low as 10^{10} cm^3 mol^{-1} s^{-1} [27]. In addition, C_4F_8 was not detected under the conditions studied, suggesting it is not produced to a significant extent. It is noted that a high activation barrier was reported by Yu et al. [28] for the transformation of *c*-C_3F_6 to C_3F_6 (R13). As no *c*-C_3F_6 was detected in the present study, it seems that this reaction does not play a major role in the formation of C_3F_6. However, with similar activation energy (210 kJ mol^{-1}) and *A* factor (10^{15} s^{-1}), Moon et al. found that this mechanism can predict the trends of C_3F_6 production and C_2F_4, as well for the pyrolysis of CHF_3 at 1173 K although the formation rate of C_3F_6 is slightly over-predicted [7]. Similarly to the present study, the intermediate, almost no *c*-C_3F_6 was also detected during their work.

$$2C_2F_4 \rightarrow C_4F_8 \quad \text{(R14)}$$

$$2C_2F_4 \rightarrow c\text{-}C_4F_8 \quad \text{(R15)}$$

$$C_4F_8 \rightarrow C_3F_6 + CF_2 \quad \text{(R16)}$$

$$c\text{-}C_4F_8 \rightarrow C_3F_6 + CF_2 \quad \text{(R17)}$$

Combining the reactions presented in Table 2 with NIST dataset, results in the development of a modified pyrolysis mechanism. This mechanism subsequently served to model the reaction system, the results of which are shown in Fig. 2. The conversion of CHF_3 and C_3F_6 formation rates predicted by modified mechanism are in good agreement with the experimental values. Although the prediction of C_2F_4 formation is improved remarkably compared with NIST mechanism, a slight over-prediction remains at high reaction temperatures. Most probably, some by-products formed at high temperatures, which are not accounted for in the model, are responsible for this difference.

4.2. Reaction of CHF_3 with CH_4

Following the study of the pyrolysis of CHF_3, the investigation focused on the reaction of CHF_3 with CH_4. Our previous studies have discovered that CHF_3 can be converted to vinyl difluoride, $CH_2{=}CF_2$, through reaction with CH_4 [8,9]. In these studies, the reactions involving the formation of a major by-product, C_2F_4 and the target product, $CH_2{=}CF_2$ were explored, and conditions which maximized $CH_2{=}CF_2$ yield were assessed. To facilitate our under-

Table 2
Modified and new reaction steps considered in modelling of CHF_3 pyrolysis[a]. For the purpose of brevity, reactions taken directly from NIST HFC mechanism are not shown in this table.

No.	Reaction	A (s^{-1} or $cm^3\,mol^{-1}\,s^{-1}$)	n	E, ($kJ\,mol^{-1}$)	Ref.
	$CHF_3 + M \rightarrow CF_2 + HF + M$	3.4×10^{30}	−4.0	288.7	NIST
Replaced by					
R2	$CHF_3 \rightarrow CF_2 + HF$	5.2×10^{13}	0	295	This study
R10	$CF_2 + CF_2{:}CF_2 \rightarrow C_3F_6$	1.6×10^{11}	0	77	[27]
R11	$CF_2{:}CF_2 + CF_2{:}CF_2 \rightarrow C_3F_6 + CF_2$	1.0×10^{12}	0	125.5	[47]
R12	$c\text{-}C_3F_6 \rightarrow CF_2{:}CF_2 + CF_2$	1.8×10^{13}	0	182.0	[48]
R13	$c\text{-}C_3F_6 \rightarrow C_3F_6$	6.8×10^{14}	0	268.8	[28]

[a] The rate coefficients of the forward reaction is $k = AT^n \exp(-E/RT)$, where A is in pre-exponential factor, E is activation energy and R is the ideal gas constant.

standing of this reaction and improve the yield of $CH_2{=}CF_2$, we attempt to elucidate the mechanism in more detail and discuss the pathways which lead to major and minor products.

4.2.1. Experimental results

The gas-phase reaction of CHF_3 with equimolar CH_4 (10% CHF_3 and 10% CH_4 with N_2 balance) was carried out in an alumina tube reactor at temperature of 873–1173 K, residence time of 0.5 s and atmospheric pressure. The major products for the reaction of CHF_3 with CH_4 are $CH_2{=}CF_2$, C_2F_4 and HF. Minor products include C_3F_6, CH_2F_2, C_2H_3F, C_2HF_3, C_2H_6, C_2H_2 and CHF_2CHF_2. Trace amounts of $CF_3CH{=}CF_2$, $CH_2{=}CFCF_3$, $C_4H_2F_2$, C_3H_8 and $CHF{=}CHF$ were also detected by GC–MS. The conversion of CHF_3 and CH_4 as a function of temperature is shown in Fig. 3. As expected, the conversion of CH_4 and CHF_3 increases with temperature, although CH_4 conversion level is always lower than that of CHF_3 under the conditions studied. Conversion of CHF_3 commences at 973 K while CH_4 conversion was observed at higher temperatures. Fig. 4 shows the formation rate of major products, $CH_2{=}CF_2$ and C_2F_4, at various temperatures. It can be seen that once conversion of CH_4 is observed, the target product, $CH_2{=}CF_2$ is initiated and similarly to the conversion of CHF_3 and CH_4, its selectivity increases significantly with temperature. Concomitant with $CH_2{=}CF_2$ formation, C_2F_4 is also formed, although a maximum formation rate of C_2F_4 is at around 1023 K, above which its rate starts to decline rapidly. The rate of formation of minor products is presented in Fig. 5. These products follow a similar rate trend to C_2F_4, achieving the highest yield at about 1150 K, except for CH_2F_2 and C_2H_2 whose formation rates increase with temperature monotonically.

Mass balances for C, H and F elements are illustrated in Table S1. Generally, balances of higher than 95% are achieved at temperatures below 1093 K. With further increase of temperature to 1173 K, C, H and F balances drop to 76%, 85% and 71% respectively. After reaction, soot and a white solid deposit are observed on the inner surface of reactor and in the alkaline scrubber. We suggest that the coke and polymer (probably poly-VDF or PTFE) are responsible for the mass losses, especially at high temperatures.

Increasing the reaction residence time from 0.1 to 0.7 s, increases the rate of formation of target product, $CH_2{=}CF_2$ from 1.5 to almost 3 mmol h^{-1} at 1173 K as shown in Fig. S1. As the residence time increases, the rate of formation of C_2H_2 also shows significant increase under the conditions studied. Formation of other minor products, such as C_2H_3F, C_2HF_3 and C_3F_6 are affected by the change of residence time to a minor extent. It is noted that the rate of C_2F_4 formation declines significantly as the residence time increases from 0.1 to 0.7 s.

In order to improve the yield of $CH_2{=}CF_2$, it is important to explore the mechanism involving its formation and less desirable reaction by-products. The mechanism of CHF_3 conversion is based on the experimental results of CHF_3 pyrolysis, although the reactions involved in the activation and initial decomposition of CH_4 remain unclear, as there should be no gas-phase decomposition of CH_4 even at 1173 K.

4.2.2. Chemical modelling and mechanistic analysis

In the absence of CH_4, the conversion of CHF_3 amounts to around 15% at 1073 K as shown in Fig. 2(a). However, with the introduction of equimolar amounts of CH_4 and CHF_3, the conversion level drops slightly to 12%, which is close to conversion levels observed for CHF_3 pyrolysis. In both pyrolysis and in the presence of CH_4, the conversion of CHF_3 commences at 973 K. Clearly, the presence of CH_4 does not facilitate the conversion of CHF_3 which suggests that there is a common primary CHF_3

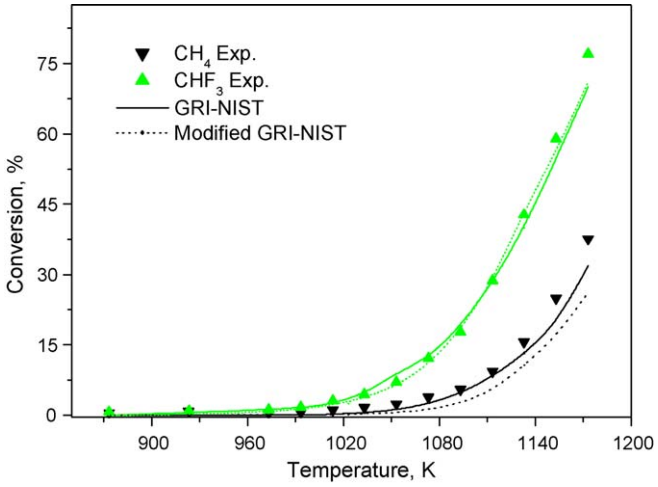

Fig. 3. Conversion of CHF_3 and CH_4 as a function of temperature during the reaction of CHF_3 with CH_4.

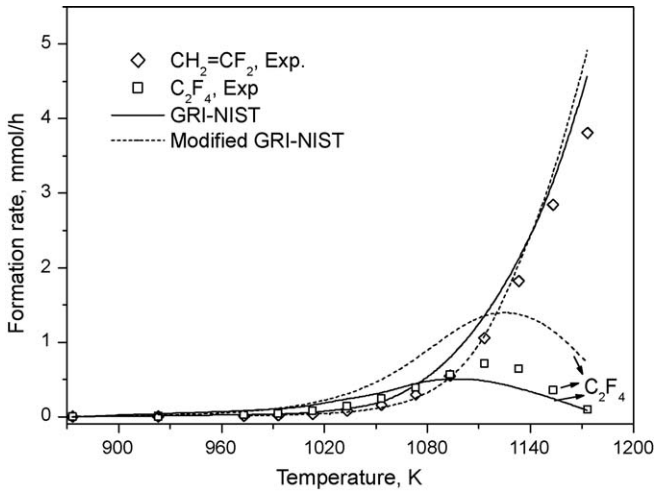

Fig. 4. Formation rate of major products as a function of temperature during reaction of CHF_3 with CH_4.

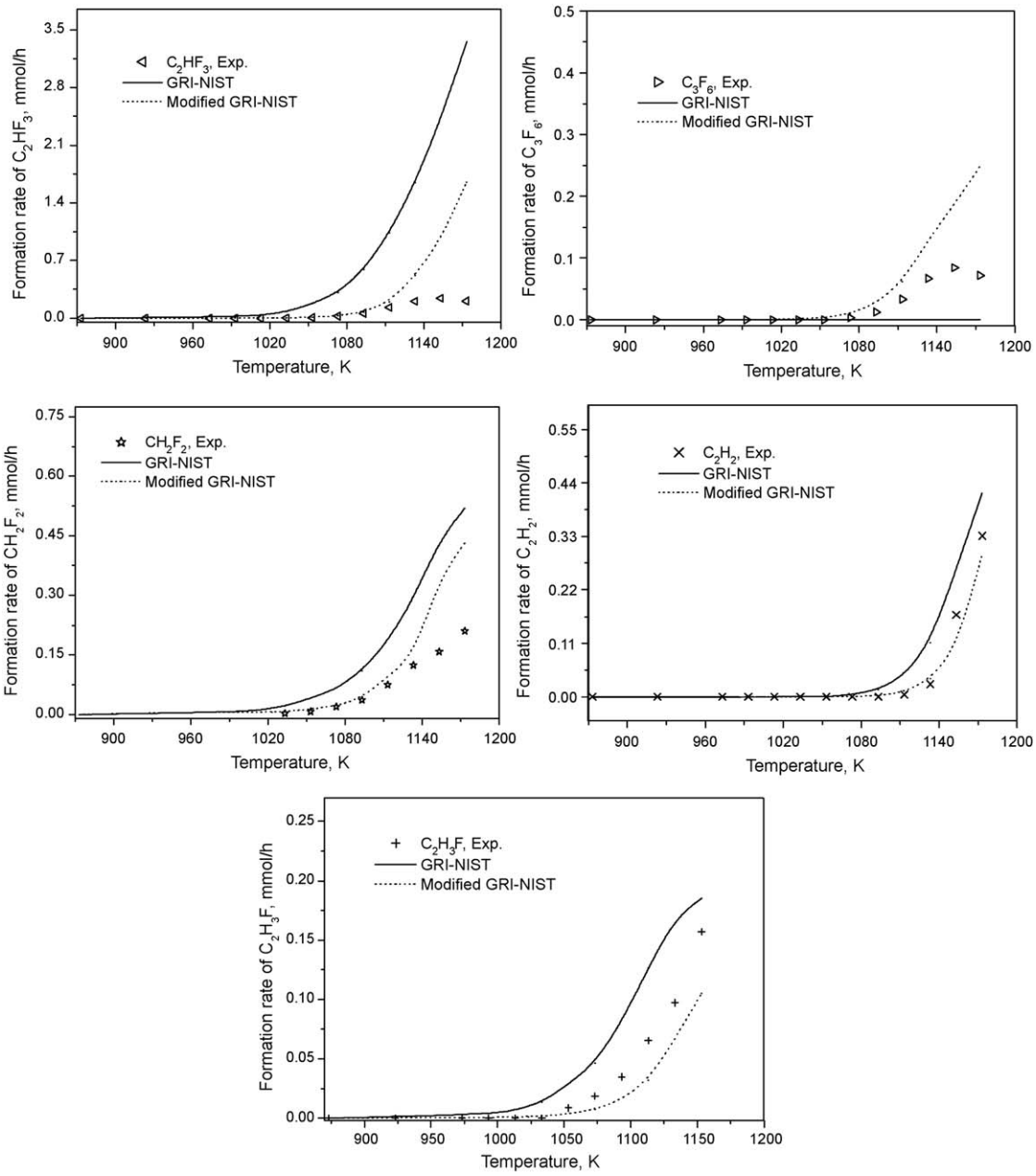

Fig. 5. Formation rate of minor products as a function of temperature during reaction of CHF_3 with CH_4.

decomposition pathway for both the processes. Similar results were found for the thermal decomposition of CHF_3 in the presence of He or H_2 [29]. We conclude that CHF_3 is inert to attacks by H_2, H or CH_4. During pyrolysis of CHF_3 and in the reaction with CH_4, the initial reaction steps involve the decomposition of CHF_3 and subsequent formation of HF and the CF_2 radical. CH_4 is unlikely to be involved in the initial steps since no significant evidence was found for its decomposition during CH_4 pyrolysis even at 1173 K [9].

Comparison of the experimental results with model predictions is shown in Figs. 3–5, including the conversion and rate of formation of major and minor products. As illustrated in Fig. 3, although the GRI-NIST model can predict the conversion of CH_4 and CHF_3 very well, it was found that there are problems associated with the rate constants of the reactions involved in CH_4 activation [8]. In the GRI-NIST mechanism, reaction pathway analysis identifies the reverse reaction of (R18) and (R20) and forward reaction (R19) as these responsible for CH_4 activation.

$$CF_3 + CHF_2 \rightarrow CF_2 + CHF_3 \quad \text{(R18)}$$

$$CF_3 + CH_4 \rightarrow CH_3 + CHF_3 \quad \text{(R19)}$$

$$CH_3 + CHF_2 \rightarrow CH_4 + CF_2 \quad \text{(R20)}$$

In contrast, Yu et al. suggests that these reactions are not likely to be responsible for CH_4 activation, since the A factor of 8×10^{14} cm^3 mol^{-1} s^{-1} is considered to be too high for the reverse reaction of (R18) [8]. In fact, the singlet CF_2 is very non-reactive since the closed-shell singlet CF_2 ($^1A_1$) is strongly stabilized by pp-back donation [30]. However, the metastable triplet CF_2 ($^3B_1$), having a rather long lifetime of about 1 s, is believed to be much more reactive and an A factor of 1.2×10^{13} cm^3 mol^{-1} s^{-1} was estimated for the reaction with CH_4 [31]. Because the triplet lies 238.1 kJ mol^{-1} above the ground-state singlet, the ratio of triplet to

singlet ground-state populations is only 8×10^{-11}, hence the reactions of the triplet can be neglected [8].

By means of *ab initio* calculations, we failed to locate a transition structure for the reverse reaction (R20). Instead, it was found that CF_2 can insert into C–H via reaction (R21) with activation energy of 163 kJ/mol. The exponential factor was estimated to be 1.5×10^{11} cm^3 mol^{-1} s^{-1}.

$$CF_2 + CH_4 \rightarrow CH_3CF_2H \quad (R21)$$

$$CH_3CF_2H \rightarrow CHF_2 + CH_3 \quad (R22)$$

With even higher activation energy (401 kJ mol^{-1}), CH_3CF_2H can further produce CH_3 and CHF_2 radicals through reaction (R22). The exponential factor of this reaction is around 1×10^{17} cm^3 mol^{-1} s^{-1} based on the analogous decomposition reaction of C_2H_6.

$$CH_3 + CF_2 \rightarrow CH_2{=}CF_2 + H \quad (R23)$$

Once CH_3 is formed, the major product, $CH_2{=}CF_2$ can be produced via reaction (R23) with CF_2, which is derived from the elimination of HF from CHF_3. This reaction has been studied using quantum chemical theory and it is found that this reaction leads to the formation of $CH_2{=}CF_2$ with an activation energy of almost zero [32]. With this discussion in mind, new reaction steps including (R21)–(R23) were introduced into the GRI-NIST mechanism, replacing (R18)–(R20). However, modelling results show that this new mechanism does not correctly predict the conversion of CH_4. Apparently, reactions (R21) and (R22) are not the primary pathways responsible for the activation of CH_4 and formation CH_3 because of their high-energy barriers. There must be other reactions playing a major role in the activation of CH_4.

It was speculated that there are reactions occurring on the surface of the reactor (α-Al_2O_3) and CH_4 activation takes place as a consequence of surface reactions [8]. In order to model the reaction system, a reaction step (R24) was included to mimic the surface reaction while CH_4 was thought to be activated by surface fluorine radicals. However, this hypothesis seems to conflict with experimental results when it was found that after packing Al_2O_3 or AlF_3 chips into the reactor, no enhanced conversion of CH_4 was observed. Furthermore, if this reaction takes place to a significant extent, the formation of CF_4 and C_2F_6 via reactions (R7), (R25) and (R26) during pyrolysis of CHF_3 is expected. However, even trace amounts of CF_4 and C_2F_6 were not detected in the present study. In addition, for the reaction of CHF_3 with CH_4, CH_3F will be the key intermediate which is also absent from the product profile.

$$CF_3 + CF_3 \rightarrow C_2F_6 \quad (R7)$$

$$CF_2 \rightarrow C + F + F \quad (R24)$$

$$CF_2 + F \rightarrow CF_3 \quad (R25)$$

$$CF_3 + F \rightarrow CF_4 \quad (R26)$$

In the previous [8] and present studies, trace amounts of H_2 were detected, although accurate determination of the amount of H_2 produced was not possible with the present analysis train. Excluding H_2, over 95% of hydrogen is balanced, which supports the assertion that the rate of formation of H_2 is low. However, it has been suggested that a relatively low concentration of H· may lead to the activation of CH_4 via a series of chain reactions ((R27)–(R31)) [33].

Initiation:

$$CH_{4(s)} \rightarrow CH_3 + H \quad (R27)$$

Propagation:

$$H + CH_4 \rightarrow CH_3 + H_2 \quad (R28)$$

$$CH_4 + CH_3 \rightarrow C_2H_6 + H \quad (R29)$$

$$CH_3 + C_2H_6 \rightarrow C_2H_5 + H \quad (R30)$$

$$C_2H_5 \rightarrow C_2H_4 + H \quad (R31)$$

To examine this hypothesis, the pyrolysis of CH_4 was investigated both experimentally and computationally. The results are shown in Table 3, together with the modelling results based on the existing GRI mechanism. Indeed, the conversion of CH_4 and subsequent formation of C_2H_6, although low, was observed with our alumina reactor. The existing GRI mechanism was used to model this reaction. Virtually no reaction was predicted under any of the conditions studied. This suggests that a small amount of CH_4 may be activated on the surface of reactor, at least at high temperatures. During the reaction of CH_4 with CHF_3, as a result of the production of HF, the reactor surface is likely to be fluorinated [34]. Hence, 0.2 g AlF_3 (having a bulk volume of 0.35 cm^3 and a surface area of 480 cm^2) was packed into the reactor to simulate this fluorinated reactor surface. As shown in Table 3, AlF_3 enhances the rate of decomposition of CH_4 significantly. Consistent with these observations, it has been noted that methane can be activated, or its conversion can be improved, in the presence of Brønsted and/or Lewis acid sites [35–38]. AlF_3 is considered a strong solid Lewis acid [39] and it may initiate chain reactions ((R27)–(R31)). Although CH_4 is stable even at 1173 K, low conversion levels still can be achieved on the surface of reactor. Based on these results, we introduce into the existing mechanisms a simplified reaction step (R27) to simulate these surface reactions. Numerous results have been reported for the kinetics of gas-phase reaction of (R27) [40,41], for which the estimated activation energy varies from 270 to 490 kJ mol^{-1}. Based on the observed effect of surface reaction on methane activation, an activation energy of 270 kJ mol^{-1} appears to be too high. Improved agreement with experimental data can be obtained by decreasing the activation energy and exponential factor to 234 kJ mol^{-1} and 1.09×10^{10} s^{-1}. After introducing this reaction into GRI mechanism, closer prediction can be obtained compared with experimental results as shown in Table 3.

Combining the other reaction steps outlined in Table 4 with the GRI-NIST mechanism, we introduce our new modified reaction

Table 3
Experimental and modelling results of pyrolysis of CH_4 as a function of temperature in an alumina tube reactor[a].

T (K)	CH_4 Pyrolysis		GRI-Mech Prediction		Modified model		CH_4 Pyrolysis over AlF_3[b]		
	Conversion (%)	C_2H_6 (mmol h^{-1})	Conversion (%)	C_2H_6 (mmol h^{-1})	Conversion (%)	C_2H_6 (mmol h^{-1})	Conversion (%)	C_2H_6 (mmol h^{-1})	C_2H_4 (mmol h^{-1})
973	0.049	0	0.002		0.002	0.00014	0.11	0.0036	0
1023	0.024	0.0026	0.004	9×10^{-7}	0.018	0.0016	0.26	0.0061	0
1073	0.018	0.0018	0.008	8.6×10^{-6}	0.098	0.009	0.68	0.01	0.002
1123	0.14	0.004	0.02	7×10^{-5}	0.46	0.04	0.37	0.011	0.005
1173	0.31	0.013	0.04	0.0005	0.83	0.011	1.1	0.027	0.009

[a] At pressure of 1.01 bar and residence of 0.5 s.
[b] During experiment, 0.2 g AlF_3 was packed into the reactor. Other reaction conditions remained unchanged.

Table 4
Modified and new reaction steps considered in modelling of reaction of CHF_3 with CH_4[a]. For the purpose of brevity, reactions taken directly from NIST HFC mechanism are not shown in this table.

No.	Reaction	A (s^{-1} or $cm^3\,mol^{-1}\,s^{-1}$)	n	E ($kJ\,mol^{-1}$)	Ref.
	$CHF_3 + M \rightarrow CF_2 + HF + M$	3.4×10^{30}	−4.0	288.7	NIST
Replaced by					
R2	$CHF_3 \rightarrow CF_2 + HF$	5.2×10^{13}	0	295	This study
R10	$CF_2 + CF_2{:}CF_2 \rightarrow C_3F_6$	1.6×10^{11}	0	77	[27]
R11	$CF_2{:}CF_2 + CF_2{:}CF_2 \rightarrow C_3F_6 + CF_2$	1.0×10^{12}	0	125.5	[47]
R12	$c\text{-}C_3F_6 \rightarrow CF_2{:}CF_2 + CF_2$	1.8×10^{13}	0	182.0	[48]
R13	$c\text{-}C_3F_6 \rightarrow C_3F_6$	6.8×10^{14}	0	268.8	[28]
R20	$CHF_2 + CH_3 \rightarrow CF_2 + CH_4$	3.0×10^{13}	0	3.4	
Replaced by					
−R20	$CH_4 + CF_2 \rightarrow CH_3 + CHF_2$	1.0×10^{13}	0	159.5	[8]
R21	$CH_4 + CF_2 \rightarrow CH_3CF_2H$	1.5×10^{11}	0	163	This study
R22	$CH_3CF_2H \rightarrow CH_3 + CHF_2$	1.0×10^{17}	0	401	This study
R23	$CH_3 + CF_2 \rightarrow CH_2CF_2 + H$	6.0×10^{12}	0	14.6	
Change to					
		2.1×10^{13}	−0.2	0	[32]
R27	$CH_4 \rightarrow H + CH_3$	1.09×10^{10}	0	234	This study
R34	$CHF_2 + CF_2 \rightarrow CF_2{:}CF_2 + H$	2.0×10^{12}	0	14.6	
Replaced by					
−R34	$CF_2{:}CF_2 + H \rightarrow CHF_2 + CF_2$	8.4×10^{8}	1.5	19.2	This study

[a] The rate coefficients of the forward reaction is $k = AT^n \exp(-E/RT)$, where A is in pre-exponential factor, E is activation energy and R is the ideal gas constant.

mechanism. The reaction parameter for CHF_3 decomposition is obtained from our pyrolysis study. Relatively good agreement between model predictions and experimental results are achieved, as shown in Figs. 3–5, although among the products, C_2HF_3 and C_3F_6 are significantly over-predicted by the modelling. We suggest this is due to the absence of reactions steps which lead to the decomposition of these two species. For example, significant amounts of soot were observed during the experiments, while only trace amounts of carbon were predicted from modelling.

With this modified mechanism, sensitivity analysis for the concentration of CH_3 was performed and the results are shown in Fig. 6. Sensitivity analysis is often used to describe the dependence of rate of formation of a certain species on the reactions involved in the mechanism. By comparing sensitivity coefficients, the rate-determining and other most important reactions for formation of different species can be identified and analyzed quantitatively. A more detailed example can be seen in Reference [42].

Clearly, the sensitivity analysis further confirms our suggestion of the major pathways for activation of CH_4. Although almost no CH_4 conversion was observed without reaction (R27), sensitivity of this reaction to CH_3 concentration is extremely low. This indicates that the primary role for reaction (R27) is that it acts as an initiator for the conversion of CH_4.

Initiation:

$$CH_{4(s)} \rightarrow \cdot CH_3 + H\cdot \quad \text{(R27)}$$

Propagation:

$$H + CF_2{:}CF_2 \rightarrow CHF_2CF_2 \quad \text{(R32)}$$

$$H + CF_2{:}CF_2 \rightarrow CHFCF_2 + F \quad \text{(R33)}$$

$$CHF_2 + CF_2 \rightarrow H + CF_2{:}CF_2 \quad \text{(R34)}$$

$$CHF_2CF_2 + CH_4 \rightarrow CHF_2CHF_2 + CH_3 \quad \text{(R35)}$$

$$F + CH_4 \rightarrow CH_3 + HF \quad \text{(R36)}$$

$$H + CH_4 \rightarrow CH_3 + H_2 \quad \text{(R37)}$$

$$CH_3 + CF_2 \rightarrow CH_2{=}CF_2 + H \quad \text{(R23)}$$

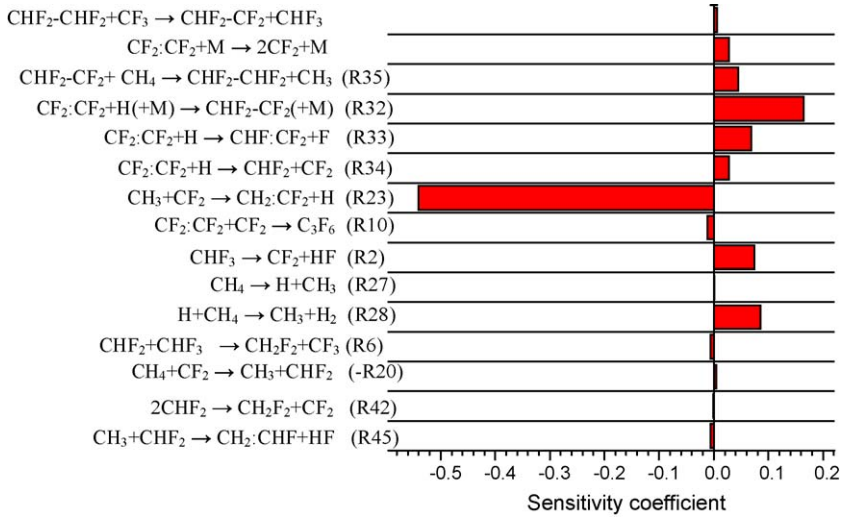

Fig. 6. Sensitivity analysis of reactions to the concentration of CH_3 radical at temperature 1113 K, pressure of 1.01 bar and residence time of 0.5 s.

As shown in Fig. 6, CH_3 consumption is dominated by reaction (R23), forming the target product, CH_2=CF_2. In reaction (R23), CF_2 is formed via reaction (R2) which is the major channel for the decomposition of CHF_3 (see Fig. S2).

For the NIST-GRI mechanism, the major reaction step leading to the formation of C_2HF_3 involves the coupling of CHF_2 and CF_2 via reaction (R38). Although no literature references for this reaction have been found, kinetic data in the NIST-GRI mechanism is consistent with the results of similar reactions, which have been investigated both experimentally and computationally [43]. We suggest that the final estimation of the concentration of C_2HF_3 is over-predicted because of the relatively high concentration of CHF_2 predicted in the model.

$$CHF_2 + CF_2 \rightarrow CHF : CF_2 + F \quad (R38)$$

Reaction pathway analysis indicates that the main pathway to CHF_2 formation is via the reverse reaction of (R34). Its second-order rate constant is estimated to be greater than 6×10^{-8} cm^3 mol^{-1} s^{-1} at 1093 K, based on the modelling data, although much lower values were reported [44–46] for this reaction based on the experimental observation. To improve the prediction of C_2HF_3, (R34) was replaced by (−R34) in the modified mechanism. The activation energy is assumed to be 19 kJ mol^{-1}, which is equal to the standard enthalpy changes of (−R34), which is lower than the activation energy barrier.

There are a number of uncertainties in elucidating the pathways for formation of C_3F_6, which is generally thought to be formed via reaction of C_2F_4 with CF_2 [27,28]. The reaction between CF_2 and C_2F_4 was studied using the *meta* hybrid density functional theory method of BB1K, which showed that the addition of CF_2 to C_2F_4 invariably leads to the formation of *c*-C_3F_6, although no transition state leading directly to C_3F_6 was found [28]. In the present experiments, no *c*-C_3F_6 was detected, which suggests the NIST-GRI mechanism may not include all pathways leading to the formation of C_3F_6. As a consequence, significant discrepancies were found between the prediction and experimental results of C_3F_6. In order to model the formation of C_3F_6, reactions (R10)–(R14) are included in the modified mechanism, which result in reasonable agreement with experiments during the pyrolysis of CHF_3.

Based on the suggested mechanism, major channels to other products can be obtained.

Channel to C_2H_6:

$$2CH_3 \rightarrow C_2H_6 \quad (R39)$$

Channels to CH_2F_2:

$$CHF_2 + CH_4 \rightarrow CH_2F_2 + CH_3 \quad (R40)$$

$$CHF_3 + CHF_2 \rightarrow CH_2F_2 + CF_3 \quad (R41)$$

$$2CHF_2 \rightarrow CH_2F_2 + CF_2 \quad (R42)$$

Channels to C_2H_3F:

$$CH_4 + CF_2 \rightarrow CH_2 : CHF + HF \quad (R43)$$

$$CH_4 + CF \rightarrow CH_2 : CHF + H \quad (R44)$$

$$CH_3 + CHF_2 \rightarrow CH_2 : CHF + HF \quad (R45)$$

$$CH_2{=}CF_2 + H \rightarrow CH_2 : CHF + F \quad (R46)$$

Channels for CHF_2CHF_2:

$$2CHF_2 \rightarrow CHF_2CHF_2 \quad (R47)$$

$$CHF_2CF_2 + H \rightarrow CHF_2CHF_2 \quad (R48)$$

$$CHF_2CF_2 + CH_4 \rightarrow CHF_2CHF_2 + CH_3 \quad (R35)$$

5. Conclusions

The pyrolysis of CHF_3 and reaction of CHF_3 with CH_4 have been investigated experimentally and computationally. It was found that CHF_3 pyrolysis commences around at 973 K at residence time of 0.5 s, and its conversion increases with temperature. The products identified by GC–MS include C_2F_4, C_3F_6 and trace amounts of C_2HF_3. The overall rate of CHF_3 decomposition can be expressed as $5.2 \times 1013\,[s^{-1}]\,e^{-295[kJ\,mol^{-1}]/RT}$. The NIST mechanism predicts C_2F_4 as the only carbon containing species, with its formation rate over-predicted significantly at temperatures above 1093 K. Another major reaction product, C_3F_6 is not included in the mechanism. A modified mechanism was developed which can reproduce experimental data reasonably well.

For the reaction of CHF_3 with CH_4, the major products are CH_2=CF_2, C_2F_4 and HF. Minor products include C_3F_6, CH_2F_2, C_2H_3F, C_2HF_3, C_2H_6, C_2H_2 and CHF_2CHF_2. Trace amounts of CF_3CH=CF_2, CH_2=$CFCF_3$, $C_4H_2F_2$, C_3H_8 and CHF=CHF were also detected by GC–MS. Predictions based on the GRI-NIST mechanism show good agreement between experiments and modelling for the conversion of CHF_3 and CH_4, but significant discrepancies were observed for the selectivity of some reaction products. Modifications to the existing GRI-NIST mechanism are suggested and when incorporated in the model, significantly improve agreement between experiments and modelling. Based on mechanistic pathway analysis, the initial step in the decomposition of CHF_3 includes the formation of CF_2 radical and HF. This reaction dominates the pyrolysis of CHF_3 and reaction of CHF_3 with CH_4. Trace amounts of CH_4 decompose on the surface of reactor, producing H radical. It is proposed that CH_4 is activated by a series of chain reactions which are initiated by this small amount of H radicals.

Acknowledgements

The Australian Research Council is gratefully acknowledged for financial support for this project. W.H. is indebted to the Department of Education, Science and Training (DEST) of the Australian Government and the University of Newcastle, Australia for postgraduate scholarships.

Appendix A. Supplementary data

Supplementary data associated with this article can be found, in the online version, at doi:10.1016/j.jfluchem.2010.03.012.

References

[1] Production and Consumption of Ozone Depleting Substances Under the Montreal Protocol, UNEP, 2008 Available at http://ozone.unep.org/Data_Reporting/Data_Access/.
[2] D.W.F. Guus, J.M. Velders, J.S. Daniel, M. McFarland, S.O. Andersen, Proc. Nat. Acad. Sci. 106 (2009) 10949–10954.
[3] D.E. Oram, W.T. Sturges, S.A. Penkett, A. McCulloch, P.J. Fraser, Geophys. Res. Lett. 25 (1998) 35–38.
[4] AM0001: Incineration of HFC 23 Waste Streams, UNFCCC, 2006 http://cdm.unfccc.int/methodologies/index.html.
[5] W.B. Feaver, J.A. Rossin, Catal. Today 54 (1999) 13–22.
[6] H. Onoda, T. Ohta, J. Tamaki, K. Kojima, Appl. Catal. A 288 (2005) 98–103.
[7] D.J. Moon, M.J. Chung, H. Kim, Y.S. Kwon, B.S. Ahn, Ind. Eng. Chem. Res. 41 (2002) 2895–2902.
[8] H. Yu, E.M. Kennedy, J.C. Mackie, B.Z. Dlugogorski, Environ. Sci. Technol. 40 (2006) 5778–5785.
[9] W.F. Han, H. Yu, E.M. Kennedy, J.C. Mackie, B.Z. Dlugogorski, Environ. Sci. Technol. 42 (2008) 5795–5799.
[10] A.L. Moore, Fluoroelastomers Handbook: the Definitive User's Guide and Databook, William Andrew Publishing, Norwich, 2005.
[11] M. Visca, M.S. Kelly, B.L. Kent, EP 1679352 (2007).
[12] H. Yu, E.M. Kennedy, M.A. Uddin, A.A. Adesina, B.Z. Dlugogorski, Catal. Today 97 (2004) 205–215.

[13] K. Li, E.M. Kennedy, B.Z. Dlugogorski, Ind. Eng. Chem. Res 38 (1999) 3345–3352.
[14] M.J. Height, E.M. Kennedy, B.Z. Dlugogorski, J. Chromatogr. A 841 (1999) 187–195.
[15] Softpredict, Cosilab Collection, Version 2.1.0 ed., Rolexo-Softpredict-Cosilab GmbH & Co KG, Bad Zwischenahn, Germany, 2007, www.Softpredict.com.
[16] A. Manion, R.E. Huie, R.D. Levin, D.R. Burgess Jr., V.L. Orkin, W. Tsang, W.S. McGivern, J.W. Hudgens, V.D. Knyazev, D.B. Atkinson, E. Chai, A.M. Tereza, C.-Y. Lin, T.C. Allison, W.G. Mallard, F. Westley, J.T. Herron, R.F. Hampson, D.H. Frizzell, NIST Chemical Kinetics Database, NIST Standard Reference Database 17, Version 7.0 (Web Version) Release 1.4.3, Data Version 2008.12, National Institute of Standards and Technology, Gaithersburg, MD, 2008, http://kinetics.nist.gov/.
[17] G.P. Smith, D.M. Golden, M. Frenklach, N.W. Moriarty, B. Eiteneer, M. Goldenberg, C.T. Bowman, R.K. Hanson, S. Song, W.C. Gardiner, V.V. Lissianski Jr., Z. Qin, GRI-Mech 3.0, 2008 http://www.me.berkeley.edu/gri_mech/.
[18] E. Tschuikow-Roux, J.E. Marte, J. Chem. Phys. 42 (1965) 2049–2056.
[19] E. Tschuikow-Roux, J. Chem. Phys. 42 (1965) 3639–3642.
[20] A.P. Modica, J.E. LaGraff, J. Chem. Phys. 44 (1966) 3375–3379.
[21] Y. Hidaka, T. Nakamura, H. Kawano, Chem. Phys. Lett. 187 (1991) 40–44.
[22] K.P. Schug, H.G. Wagner, F. Zabel, Ber. Bunsen-Ges. Phys. Chem. 83 (1979) 167–175.
[23] D.W. Placzek, B.S. Rabinovitch, G.Z. Whitten, E. Tschuikow-Roux, J. Chem. Phys. 43 (1965) 4071–4080.
[24] S.F. Politanskii, V.U. Shevchuk, Kinet. Catal. 9 (1968) 496–503.
[25] J.C. Biordi, C.P. Lazzara, J.F. Papp, J. Phys. Chem. 82 (1978) 125–132.
[26] F. Battin-Leclerc, A.P. Smith, G.D. Hayman, T.P. Murrells, J. Chem. Soc. Faraday Trans. 92 (1996) 3305–3313.
[27] N.N. Buravtsev, A.S. Grigor'ev, Y.A. Kolbanovskii, Kinet. Catal. 30 (1989) 21–30.
[28] H. Yu, E.M. Kennedy, W.H. Ong, J.C. Mackie, W. Han, B.Z. Dlugogorski, Ind. Eng. Chem. Res. 47 (2008) 2579–2584.
[29] R. Romelaer, V. Kruger, J.M. Baker, W.R. Dolbier, J. Am. Chem. Soc. 123 (2001) 6767–6772.
[30] S. Koda, J. Phys. Chem. 83 (1979) 2065–2073.
[31] X.J. Hou, T.L. Nguyen, S.A. Carl, J. Peeters, M.T. Nguyen, Chem. Phys. Lett. 402 (2005) 460–467.
[32] H. Yu, J.C. Mackie, E.M. Kennedy, B.Z. Dlugogorski, Ind. Eng. Chem. Res. 45 (2006) 3758–3762.
[33] C.H. Bamford, C.F.H. Tipper, in: C.F.H.T.C.H. Bamford (Ed.), Decomposition and Isomerisation of Organic Compounds, Elsevier, Amsterdam, 1972, pp. 36–64.
[34] M. Bankhead, G.W. Watson, G.J. Hutchings, J. Scott, D.J. Willock, Appl. Catal. A 200 (2000) 263–274.
[35] T. Jin, T. Yamaguchi, K. Tanabe, J. Phys. Chem. 90 (2002) 4794–4796.
[36] W. Hua, A. Goeppert, J. Sommer, Appl. Catal. A 219 (2001) 201–207.
[37] F.T.T. Ng, C.R. Rourke, J. Lynn, J.S. Kevin, E.C. Sanford, Studies in Surface Science and Catalysis, Elsevier, 1992, pp. 91–97.
[38] F.R. Chen, G. Coudurier, J.F. Joly, J.C. Vedrine, J. Catal. 143 (1993) 616–626.
[39] G. Eltanany, S. Rudiger, E. Kemnitz, J. Mater. Chem. 18 (2008) 2268–2275.
[40] W.C. Gardiner Jr., J.H. Owen, T.C. Clark, J.E. Dove, S.H. Bauer, J.A. Miller, W.J. McLean, Symp. (Int.) Combust. 15 (1975) 857–868.
[41] J.H. Kiefer, S.S. Kumaran, J. Phys. Chem. 97 (1993) 414–420.
[42] M. Forsth, Combust. Flame 130 (2002) 241–260.
[43] Y. Saso, D.L. Zhu, H. Wang, C.K. Law, N. Saito, Combust. Flame 114 (1998) 457–468.
[44] K. Sugawara, K. Okasaki, S. Sato, Bull. Chem. Soc. Jpn. 54 (1981) 358–361.
[45] E.B. Gordon, B.I. Ivanov, A.P. Perminov, V.E. Balalaev, Chem. Phys. 35 (1978) 79–89.
[46] J.P. Kilcoyne, K.R. Jennings, J. Chem. Soc., Faraday Trans. 1 (70) (1974) 379–390.
[47] B. Atkinson, V.A. Atkinson, J. Chem. Soc. (1957) 2086–2094.
[48] S.H. Bauer, S. Javanovic, Int. J. Chem. Kinet. 30 (1998) 171–177.